

12-1-2014


Distinct Conformational Behaviors of Four Mammalian Dual-Flavin Reductases (Cytochrome P450 Reductase, Methionine Synthase Reductase, Neuronal Nitric Oxide Synthase, Endothelial Nitric Oxide Synthase) Determine Their Unique Catalytic Profiles

Mohammad Mahfuzul Haque
Lerner Research Institute

Mekki Bayachou
Cleveland State University, M.BAYACHOU@csuohio.edu

Jesus Tejero
University of Pittsburgh

Claire T. Kenney
Lerner Research Institute

Naw M. Pearl
Follow this and additional works at: https://engagedscholarship.csuohio.edu/scichem_facpub
University of Michigan Medical School
 Part of the [Chemistry Commons](#)

How does access to this work benefit you? Let us know!
See next page for additional authors

Recommended Citation

Haque, Mohammad Mahfuzul; Bayachou, Mekki; Tejero, Jesus; Kenney, Claire T.; Pearl, Naw M.; Im, Sang-Choul; Waskell, Lucy; and Stuehr, Dennis J., "Distinct Conformational Behaviors of Four Mammalian Dual-Flavin Reductases (Cytochrome P450 Reductase, Methionine Synthase Reductase, Neuronal Nitric Oxide Synthase, Endothelial Nitric Oxide Synthase) Determine Their Unique Catalytic Profiles" (2014). *Chemistry Faculty Publications*. 308.
https://engagedscholarship.csuohio.edu/scichem_facpub/308

This Article is brought to you for free and open access by the Chemistry Department at EngagedScholarship@CSU. It has been accepted for inclusion in Chemistry Faculty Publications by an authorized administrator of EngagedScholarship@CSU. For more information, please contact library.es@csuohio.edu.

Authors

Mohammad Mahfuzul Haque, Mekki Bayachou, Jesus Tejero, Claire T. Kenney, Naw M. Pearl, Sang-Choul Im, Lucy Waskell, and Dennis J. Stuehr

Distinct conformational behaviors of four mammalian dual-flavin reductases (cytochrome P450 reductase, methionine synthase reductase, neuronal nitric oxide synthase, endothelial nitric oxide synthase) determine their unique catalytic profiles

Mohammad M. Haque , Mekki Bayachou , Jesus Tejero , Claire T. Kenney , Naw M. Pearl , Sang-Choul Im , Lucy Waskell and Dennis J. Stuehr

Keywords

conformational equilibrium; electron transfer; flavoprotein; kinetic model; nitric oxide

Multidomain enzymes often rely on large conformational motions to function. However, the conformational setpoints, rates of domain motions and relationships between these parameters and catalytic activity are not well understood. To address this, we determined and compared the conformational setpoints and the rates of conformational switching between closed unreactive and open reactive states in four mammalian diflavin NADPH oxidoreductases that catalyze important biological electron transfer reactions: cytochrome P450 reductase, methionine synthase reductase and endothelial and neuronal nitric oxide synthase. We used stopped-flow spectroscopy, single turnover methods and a kinetic model that relates electron flux through each enzyme to its conformational setpoint and its rates of conformational switching. The results show that the four flavoproteins, when fully-reduced, have a broad range of conformational setpoints (from 12% to 72% open state) and also vary 100-fold with respect to their rates of conformational switching between unreactive closed and reactive open states (cytochrome P450 reductase > neuronal nitric oxide synthase > methionine synthase reductase > endothelial nitric oxide synthase). Furthermore, simulations of the kinetic model could explain how each flavoprotein can support its given rate of electron flux (cytochrome *c* reductase activity) based on its unique conformational setpoint and switching rates. The present study is the first to quantify these conformational parameters among the diflavin enzymes and suggests how the parameters might be manipulated to speed or slow biological electron flux.

Introduction

The diflavin reductases transfer electrons from NADPH to a variety of one-electron acceptors [1–4]. They consist of attached NADPH, FAD and FMN binding domains [1,5] that are analogous to existing proteins: the NADPH and FAD binding domains [NADPH/FAD or ferredoxin-NADP⁺-reductase-like domain (FNR)] resemble NADP⁺-ferredoxin reductases, whereas the FMN domains are analogous to flavodoxins [1,6–8]. Either flavin cofactor can exist in three different redox states: oxidized, semiquinone (sq) and hydroquinone (hq). The electron flux through these enzymes follows a linear pathway: NADPH → FAD → FMN → final acceptors [9]. Each flavin has a unique function: the FAD accepts a hydride from NADPH and then transfers reducing equivalents to FMN one at a time [10,11]. Because the mammalian diflavin reductases stabilize their one-electron reduced (semiquinone) FMN (FMN_{sq}), only the two-electron reduced (hydroquinone) FMN (FMN_{hq}) acts as an electron donor to external acceptors and then cycles between the FMN_{sq} and FMN_{hq} forms. The diflavin reductase family includes mammalian members NADPH-cytochrome P450 reductase (CPR) [6,12], the three nitric oxide synthases (NOS) [13–15], methionine synthase reductase (MSR) [16–18] and novel reductase 1 [19], and includes bacterial members sulfite reductase [20] and flavocytochrome P450 BM3 [21,22].

Electron transfer (ET) through diflavin enzymes involves specific domain domain interactions. An interface that forms between the NADPH/FAD (FNR) and FMN domains allows the interflavin ET that forms FMN_{hq}. Crystal structures of rat and human CPRs [23,24] and the reductase domain of rat neuronal nitric oxide synthase (nNOSred) [25] show the isoalloxazine rings of the bound FAD and FMN cofactors are closely positioned for rapid ET. However, in this conformation, the FMN cofactor is buried from solvent and is incapable of performing ET with protein redox partners or artificial acceptors such as cytochrome *c*. Transition of the conformationally-closed structures to more open forms is thought to be required, as was confirmed recently for CPR [26]. Electron flux through all diflavin enzymes is thought to involve conformational shuttling between closed and open states [27–31]. Crystal structures and biophysical studies have increased our understanding of the conformationally-closed and -open states of diflavin reductases and how they may participate in catalyzing electron flux to their natural acceptor proteins or to cytochrome *c* [15,23,25–27,30,32–39]. However, it is not clear how the conformational equilibria and rates

of conformational switching relate to electron flux, or how these parameters compare among the diflavin reductases. To address this, we proposed a simple four-state kinetic model (Fig. 1) [15,34,35] that relies on cytochrome *c* reductase activity to assess electron flux through the diflavin enzymes. Under typical experimental conditions with excess NADPH and cytochrome *c*, the rate of flavin reduction or cytochrome *c* reduction (k_4) is fast and not rate-limiting [30,36,37,40,41] and so the electron flux through the diflavin enzyme is only dependent on the rates of FMN domain conformational switching (k_1 , k_{-1} , k_3 , k_{-3}) and the rate of interflavin electron transfer between the FAD and FMN cofactors (k_2). The model incorporates the one-electron redox cycling of the FMN_{hq} and FMN_{sq}, which occurs naturally during turnover, and therefore includes two temporally-separate equilibrium terms, K_{sq} and K_{hq} , which differ according to the reduction state of the FMN (FMN_{sq} versus FMN_{hq}). We define $K_{sq} = k_{-1}/k_1$ and $K_{hq} = k_{-3}/k_3$ (Fig. 1), such that higher K values indicate a greater abundance of open conformations. The equilibrium described by K_{hq} involves a conformational opening step that allows the FMN_{hq} to reduce an acceptor (in this case cytochrome *c*) and consequently become oxidized to FMN_{sq}. The equilibrium described by K_{sq} involves a conformational closing step that allows the FMN_{sq} to receive another electron from the FNR domain. For simplicity, the model assumes: (a) the interflavin electron transfer step (k_2) is irreversible; (b) the reduction of FAD by NADPH and the reduction of cytochrome *c* by FMN_{hq} (k_4 step) are rapid and irreversible steps relative to all the other kinetic steps; and (c) the conformational equilibrium setpoint is unaffected by the redox state of the FMN (i.e. $K_{sq} = K_{hq}$). We previously utilized this approach to determine estimates for the K_{hq} setpoint and rates of

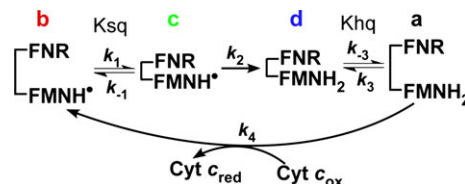


Fig. 1. Kinetic model for electron flux through a dual flavin enzyme. The model uses four kinetic rates: association (k_1 or k_3) and dissociation (k_{-1} or k_{-3}) of the FMN and FNR domains; the FMN_{hq} reduction rate (k_2) and the cytochrome *c* reduction rate (k_4). The fully reduced enzyme in the open conformation (species a) reduces cytochrome *c* and generates species b, which then undergoes successive conformational closing, interflavin electron transfer, and conformational opening steps to complete the cycle.

conformational switching and interflavin ET in the flavoprotein domains of endothelial and neuronal NOS [reductase domain of endothelial NOS (eNOSred), reductase domain of nNOS (nNOSred)] [34,36] and in site-specific variants of nNOSred [35].

In the present study, we expanded our studies to investigate CPR and MSR and we re-analyzed nNOSred and eNOSred in parallel, aiming to understand the range of conformational behaviors displayed across the mammalian dual-flavin reductase family, and how their conformational parameters may determine their different electron flux profiles. Simulations of the kinetic model show how each enzyme's unique blend of conformational equilibrium and kinetic parameters help determine its steady-state species distribution and catalytic activity. The present study provides the first measures of conformational setpoints and switching rates, which in turn have protein structural, mechanistic and functional implications.

Results

Steady-state electron flux varies widely among family members

We compared the NADPH-dependent cytochrome *c* reductase activities of the four flavoproteins at 10 and 25 °C (Table 1). Steady-state cytochrome *c* reductase activity indicates the maximal electron flux that can be achieved through the four flavoproteins because cytochrome *c* reacts quickly and irreversibly to accept an electron from their reduced FMN domains [1,15,17,27,35,36]. The reductase activities that we obtained matched with earlier reports [17,27,35,36] and, at either temperature, gave a rank order of CPR > nNOSred > eNOSred = MSR that spanned almost two orders of magnitude. This difference became the premise for the present study.

Table 1. Steady state cytochrome *c* reductase activities of dual flavin reductases. The cytochrome *c* reductase activities were determined at 25 and 10 °C as described in the Experimental procedures. The values are the mean \pm SD of three measurements carried out under identical conditions, using two different protein preparations for each enzyme. Activities of nNOSred and eNOSred were measured under CaM free conditions.

Proteins	10 °C (min ⁻¹)	25 °C (min ⁻¹)
eNOSred	27 \pm 2.3	68 \pm 6
nNOSred	474 \pm 29	752 \pm 42
CPR	1680 \pm 160	3629 \pm 290
MSR	37 \pm 3	56 \pm 4.2

Conformational K_{eq} setpoints vary among the fully-reduced flavoproteins

We estimated the conformational K_{hq} setpoints ([open-reactive]/[closed-unreactive]) of each fully-reduced flavoprotein by monitoring its reaction with an excess of cytochrome *c* in a stopped-flow spectrophotometer, as done previously [35,36]. Under our particular experimental conditions (final cytochrome *c* concentration was 50 μ M after mixing, second-order rate constant of $4.5 \times 10^6 \text{ M}^{-1} \cdot \text{s}^{-1}$ at 10 °C), the portion of reduced enzyme molecules that are in a cytochrome *c* reactive conformation (which we define as an open conformation) will transfer an electron from FMN_{hq} to cytochrome *c* at approximately 225 s⁻¹, and thus this reaction will occur almost within the instrument mixing dead time (approximately 4 ms). In contrast, the portion of enzyme molecules that exist in a cytochrome *c* unreactive conformation (which we define as closed conformation) will only reduce cytochrome *c* gradually and in relation to the rate of conformational opening. Thus, the extent to which reduction of the first molar equivalent of cytochrome *c* exhibits a fast reduction (approximately within the mixing dead-time) versus a slower reduction indicates what proportion of the fully-reduced enzyme molecules were in an open versus closed conformational state at the time of mixing, and gives an estimate for the conformational K_{hq} of the fully-reduced enzyme [34–36].

We rapid-mixed the reduced, NADPH-bound forms of each flavoprotein with an excess (100 μ M) of cytochrome *c* in the stopped-flow spectrometer under anaerobic conditions at 10 °C, and monitored the increase in A_{550} during the first few electron transfers to cytochrome *c* (i.e. the first few turnovers). Traces that were averaged from six to eight consecutive mixing reactions are shown in Fig. 2. Initial absorbance readings for $t = 0$ were determined by rapid-mixing the enzyme-free reaction buffer with the cytochrome *c* reaction solution. The experimental data are plotted in terms of the increase in absorption from the $t = 0$ point (a value designated as 0 on the left *y*-axis in Fig. 2, all panels). The right *y*-axis of each panel in Fig. 2 indicates the moles of cytochrome *c* reduced per mole of total flavoprotein that was present in each reaction. The blue dotted box indicates the absorbance change that occurred and the time that elapsed during reduction of the first molar equivalent of cytochrome *c*.

In all four enzyme reactions, we observed an initial burst phase that was followed by a slower and almost linear rate of cytochrome *c* reduction, as we had observed previously for nNOSred and eNOSred under

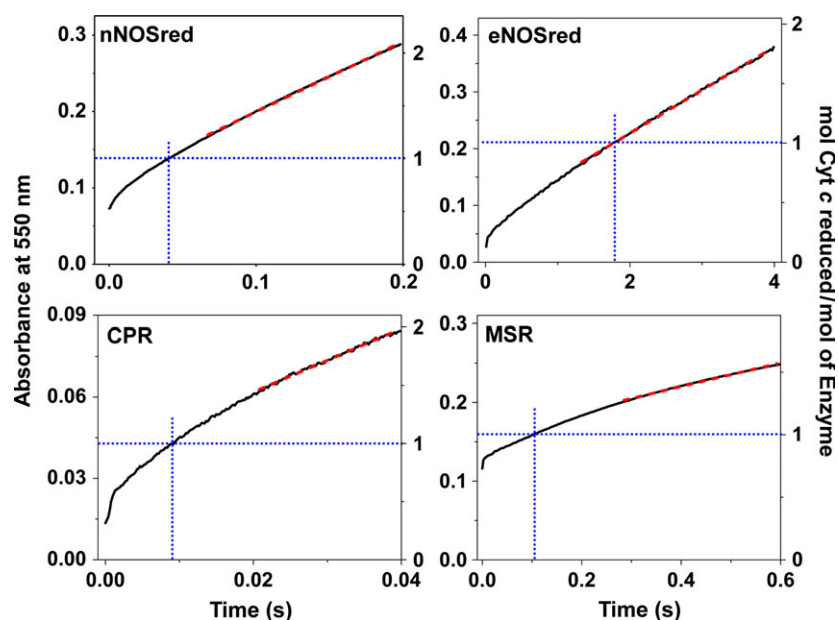


Fig. 2. Reaction of fully reduced flavoproteins with excess cytochrome *c*. Solutions of pre reduced proteins (approximately 10–12 μM) containing 200 μM NADPH were rapidly mixed with excess cytochrome *c* (100 μM) in a stopped flow instrument under anaerobic conditions at 10 °C. Kinetic traces were recorded at 550 nm during the first few electron transfers to cytochrome *c*. This was carried out for nNOSred, eNOSred, CPR and MSR. The absorbance change representing the first turnover is shown by blue dotted lines according to the right hand scale. To calculate slope, tangent lines drawn onto the near linear portions of the stopped flow traces (indicated as red dashed lines). Data are representative of at least two experiments.

similar reaction conditions [34–36]. This behavior suggests the transition to steady-state cycling already occurred within the first few turnovers in all four flavoprotein reactions. This concept was supported by our finding that the enzyme activity calculated from a tangent line drawn onto each kinetic trace within the time taken to reduce the first two equivalents of cytochrome *c* (tangents are indicated as red dashed lines in Fig. 2) essentially matched the steady-state activity that was determined for each flavoprotein in a standard steady-state assay run in a cuvette for 3 min at 10 °C (Tables 2 and 3).

The data shown in Fig. 2 suggest that the reduced diflavin enzymes have different conformational equilibrium setpoints (K_{hq}). For example, in Fig. 2 (upper left), the $t = 0$ value of the nNOSred absorbance trace, relative to the y -axis intercept of the blue dashed line, shows that approximately 50% of the first equivalent

of cytochrome *c* became reduced within the mixing dead time and the remaining 50% of the first equivalent became reduced during the subsequent observable period (within the dotted blue box). This implies the NADPH-bound, fully-reduced nNOSred molecules equally populated the open reactive and closed unreactive conformations at the time of mixing (species *a* and *d* in Fig. 1, respectively), giving an estimated $K_{\text{hq}} = 1$ for the calmodulin (CaM)-free, NADPH-bound, fully-reduced nNOSred, which matches with our previous K_{hq} estimate for nNOSred [35,36]. The situation drastically differed for eNOSred (Fig. 2, upper right). In this case, only approximately 11% of the absorbance change occurred in the instrument dead time during reduction of the first equivalent of cytochrome *c*, leaving approximately 89% of the absorbance change to be observable. This indicates the CaM-free, NADPH-bound, fully-reduced eNOSred predominantly populates the closed unreactive conformation, according to estimated K_{hq} of approximately 0.12, again similar to our earlier study [34,36].

For the NADPH-bound, fully-reduced CPR (Fig. 2, lower left), the trace showed that 33% of the first equivalent of cytochrome *c* was reduced within the instrument mixing dead time, indicating that CPR also favors the closed unreactive conformation according to $K_{\text{hq}} = 0.5$. In contrast, the NADPH-bound, fully-reduced MSR (Fig. 2, lower right) completed most of its first turnover within the mixing dead time of the instrument, leaving only approximately 28% of the first turnover observable, and giving an estimated $K_{\text{hq}} = 2.6$. Thus, the four flavoproteins displayed a

Table 2. Summary of results from reactions mixing dual flavin reductases with excess cytochrome *c*. An excess of cytochrome *c* was mixed with fully reduced proteins in a stopped flow instrument at 10 °C as described in the Experimental procedures.

Protein	Time (first turnover)	Fraction open	Fraction closed	K_{hq}	Steady state electron flux (min ⁻¹)
eNOSred	1.8 s	0.11	0.89	0.125	29.5
nNOSred	40 ms	0.51	0.49	1.04	486
CPR	9 ms	0.33	0.67	0.5	1620
MSR	117 ms	0.72	0.28	2.57	42

Table 3. Kinetic parameters derived from fitting the experimental traces according to the four state kinetic model. For details, see text. Data are representative of two or three trials with each protein. Values in parentheses are experimental values.

Protein	Measured K_A	Best fit $k_1 \quad k_3 \text{ (s}^{-1}\text{)}$	Best fit $k_{-1} \quad k_{-3} \text{ (s}^{-1}\text{)}$	Best fit $k_2 \text{ (s}^{-1}\text{)}$	Fitted steady state electron flux (s^{-1}) (experimental value)	Fitted time required for first turnover (experimental value)
eNOSred	0.125	5	0.63	5	0.49 (0.45)	1.76 (1.8) s
nNOSred	1.0	53	53	22	8.1 (7.9)	38 (40) ms
CPR	0.5	460	230	52	27 (28)	9 (9) ms
MSR	2.57	8	20.5	2.8	0.7 (0.62)	114 (117) ms

range of conformational K_{hq} setpoints in their NADPH-bound, fully-reduced states, according to the rank order: MSR > nNOSred > CPR > eNOSred (Table 2). MSR predominantly populated a reactive open conformation, nNOS was poised equally between the reactive open and unreactive closed conformations, and CPR and eNOS predominantly populated an unreactive closed conformation.

Rates of conformational switching and interflavin ET differ among the four flavoproteins

To derive rate estimates for the conformational transitions between the open reactive and closed unreactive states, and to derive an estimated rate of interflavin ET in each flavoprotein, we used computer simulations to fit the observed kinetic traces of cytochrome *c* reduction in Fig. 2 according to the four-state kinetic model in Fig. 1 that links the rates of conformational motions and interflavin ET to the electron flux to cytochrome *c* [34]. We previously used the same approach to derive rate estimates for nNOSred, nNOSred mutants and eNOSred [34,35].

In the present study, we incorporated the estimated K_{hq} values derived above into the simulations and then used an iterative method to find rate pairs for interflavin ET (k_2) and FMN domain conformational transitions (k_1, k_{-1}, k_3, k_{-3}) that support the experimentally-observed rate of electron flux to cytochrome *c* for each flavoprotein [34,35]. This analysis generated combinations of rate pairs that can each support the observed steady-state electron flux rate for each enzyme, with the general relationship being that faster rates of interflavin ET can pair with slower rates of FMN conformational switching and vice versa. The traces in the graphs of Fig. 3 indicate the allowable rate pairs for each enzyme that we derived from this fitting process. This analysis is instructive because it indicates the lower rate boundaries for the interflavin ET and the conformational opening and closing steps in each enzyme [34,35]. For example, the horizontal blue tan-

gent line drawn in the nNOSred panel of Fig. 3 (upper left) indicates the lowest boundary rate of conformational switching (17 s^{-1}) that would be able to maintain the observed electron flux to cytochrome *c* (approximately 8 s^{-1} for nNOSred at 10°C), when paired with a comparatively fast rate of interflavin ET. Similarly, a vertical blue tangent line indicates the lowest boundary rate for interflavin ET (k_2 approximately 20 s^{-1}) that would still be able to maintain the experimentally observed electron flux, when paired with a very fast rate of conformational switching. Because the conformational K_{hq} is 1 in nNOSred, $k_1 = k_{-1} = k_3 = k_{-3}$, and so only one lower boundary rate value is needed to describe all four of the conformational opening and closing steps in the kinetic model. However, for the three other flavoproteins, their conformational K_{hq} values are either greater or < 1 , and so stipulate that $k_1 \neq k_{-1}$ and $k_3 \neq k_{-3}$. Thus, two distinct lower boundary values are derived in this case that describe the conformational opening and closing rates (indicated by the blue lines in the main panels and in the insets in Fig. 3).

To obtain the best-fit rate pair values for each flavoprotein, we incorporated as an additional fitting parameter the elapsed time that was needed by each enzyme to reduce the first equivalent of cytochrome *c* [34,35] (obtained from the data in Fig. 2 as discussed above). These simulations provided a best-fit rate pair for each enzyme, whose values are marked by a blue or black box on each trace in Fig. 3, and they are listed in Table 3. The simulated kinetic traces of cytochrome *c* reduction for each enzyme, using these best-fit rate values, are overlaid with the actual experimental traces in Fig. 4, and show that a reasonable fit was obtained in each case. Together, the analysis suggests that the rates of conformational switching differ by over two orders of magnitude among the four diflavin reductases, according to rank order: CPR > nNOSred > MSR > eNOSred, whereas their corresponding rates of interflavin ET range over one order of magnitude according to the same rank order.

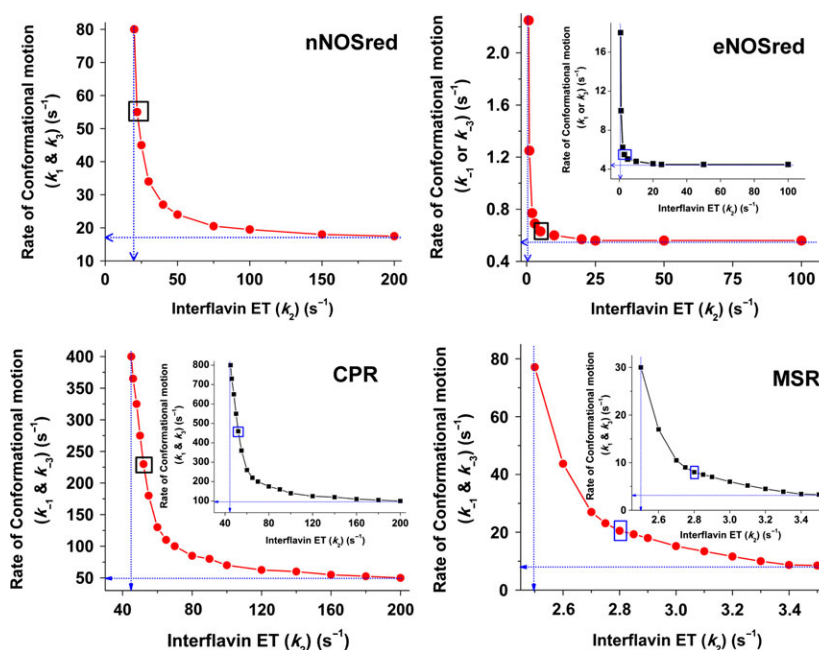


Fig. 3. Conformational motion and interflavin electron transfer rate settings that support observed electron flux through dual flavin enzymes. Data were obtained from simulations of the kinetic model in Fig. 1. For a given k_2 value, rates of conformational motion were screened for a value that yielded the observed electron flux. Blue dotted lines indicate the lower boundary values for the rates of conformational motion (y intercept) and interflavin electron transfer (x intercept). For eNOSred, CPR and MSR, the main panel shows the resulting values in terms of the conformational opening rates (k_1 – k_3). Inset: the same data points are plotted, this time indicating the rates of conformational closing (k_1 – k_3) on the y axis. The boxed points indicate the best fit rate pairs. For nNOSred, rates of conformational motion were screened for a given k_2 value that yielded an electron flux of approximately 8 s^{-1} when $K_{\text{eq}} = 1$ and $k_1 = k_3$. In eNOSred, conformational motion rates were set so that $K_{\text{h}} K_{\text{s}} = 0.125$ and the electron flux equaled 0.49 s^{-1} . For CPR to achieve an electron flux of 28 s^{-1} and a K_{eq} of 0.5, a number of k_2 values were simulated in combination with different conformational motion rates. For MSR, rates of conformational motion were screened for a corresponding k_2 value that yielded an electron flux of 0.7 s^{-1} , while $K_{\text{h}} K_{\text{s}} = 2.6$, $k_1 = k_3$ and $k_1 = k_3$.

The approach to and the final steady-state distributions of enzyme species differ among the flavoproteins

The simulations can also predict how the four enzyme conformational/redox species noted in the kinetic model (species a–d in Fig. 1) populate as each fully-reduced flavoprotein (species d + a) reacts with excess cytochrome *c* as depicted in the Fig. 2 kinetic traces. Figure 5 shows how the species distribution changes with time in all four enzymes. The kinetics of redistribution differ broadly among the flavoproteins as a direct consequence of their different rates of conformational transitions and interflavin ET. Also, only the eNOSred achieves a steady-state species distribution before the first equivalent of cytochrome *c* is reduced (time point indicated by a dotted vertical line in Fig. 5), whereas the three other flavoproteins only approach their steady-state distributions within the time needed to reduce the first equivalent. All four enzymes also have unique steady-state species distributions, as indicated

by the pie graphs in Fig. 5, as well as in Fig. 6. None of the four flavoproteins build up as the conformationally-open $\text{FMN}_{\text{h}}^{\text{q}}$ species (species a) during catalysis because this species reacts so quickly with the cytochrome *c*, although there are significant differences in the build up of species b, c, and d. For example, the fast conformational transitions in CPR cause its closed $\text{FMN}_{\text{s}}^{\text{q}}$ species (species c) to build up because the subsequent interflavin ET step is relatively slow. In contrast, eNOSred predominantly builds up as its closed $\text{FMN}_{\text{h}}^{\text{q}}$ species d because it opens relatively slowly to react with cytochrome *c*. The MSR and nNOSred both build up mainly as their open $\text{FMN}_{\text{s}}^{\text{q}}$ species b, primarily because their conformational K_{s} values provide a relatively poor driving force for the open form to transition to the closed form, as is required for the $\text{FMN}_{\text{s}}^{\text{q}}$ to be reduced. These properties also determine what percentage of $\text{FMN}_{\text{s}}^{\text{q}}$ versus $\text{FMN}_{\text{h}}^{\text{q}}$ should be present in each flavoprotein during its steady-state reaction with cytochrome *c* (Fig. 7). The eNOSred is predicted

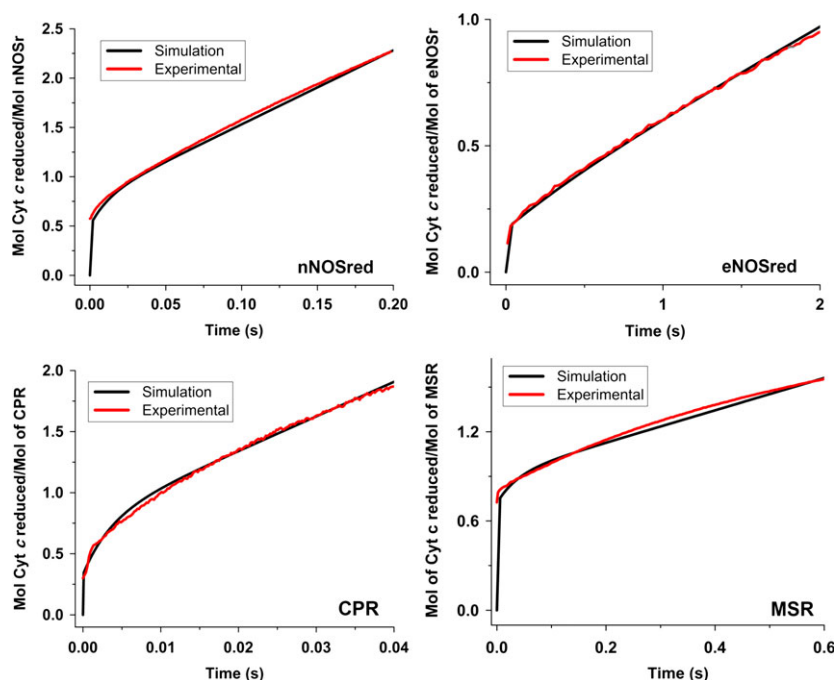


Fig. 4. Simulated reactions of fully reduced dual flavin enzymes with excess cytochrome *c*. The traces were obtained by simulating the kinetic model in Fig. 1, using different rates of conformational motion and interflavin electron transfer (k_2) to match experimental traces for each of the four dual flavins under study. Total protein concentration is 1.0 and the concentration of enzyme species *d* + *a* was set equal to 1.0 at $t = 0$ in the simulations. For nNOSred, conformational motion rates were set so that $K_{\text{hq}}/K_{\text{sq}} = 1$ and $k_1/k_3 = k_1/k_3$. With these parameters, the closest match to the experimental traces in Fig. 2 was found when $k_1/k_3 = k_3/k_3 = 53$ and $k_2 = 22$. For eNOSred, conformational motion rates were set so that $K_{\text{hq}}/K_{\text{sq}} = 0.125$, $k_1/k_3 = k_3/k_3$ and $k_1/k_3 = 0.125 \times k_1$. The best fit of experimental traces was found when the kinetic settings (s^{-1}) were $k_1/k_3 = 5.0$, $k_1/k_3 = 0.63$, $k_2 = 5.0$. In the case of CPR, the conformational motion rates were set so that $K_{\text{hq}}/K_{\text{sq}} = 0.5$, k_1/k_3 and $k_1/k_3 = 0.5 \times k_1$. The best fit was found when the kinetic settings (s^{-1}) were $k_1/k_3 = 460$, $k_1/k_3 = 230$, $k_2 = 52$. For MSR, conformational motion rates were $K_{\text{hq}}/K_{\text{sq}} = 2.57$ and k_1/k_3 ; $k_1/k_3 = 2.57 \times k_1$. The best fit was found when the kinetic settings (s^{-1}) were $k_1/k_3 = 8$, $k_1/k_3 = 20.5$, $k_2 = 2.8$. Simulated traces (black lines) are overlaid with experimental traces (red lines).

to contain 80% FMN_{hq} as a result of its build up primarily as the closed reduced species *d* during catalysis. In marked contrast, the CPR, MSR and nNOSred are predicted to contain between 80 and 95% FMN_{sq} during their steady-state reactions. The difference between eNOSred and MSR is particularly striking because they have nearly equivalent slow cytochrome *c* reductase activities (Table 1). Thus, their electron flux rates are similarly limited but for opposite reasons: eNOS has slow opening when it is in the reduced (FMN_{hq}) closed form, whereas MSR has slow closing when it is in the oxidized (FMN_{sq}) open form.

Discussion

Translating the cytochrome *c* reduction data to enzyme conformational parameters

It is important to note that our stopped-flow experiments measured the reactivity of the reduced FMN

domains (FMN_{hq}) toward cytochrome *c*, and did not directly measure specific changes in the protein conformation. Thus, linking our data to flavoprotein structural changes depends on two assumptions. First, that the FMN_{hq} is unreactive toward cytochrome *c* when the enzyme is in a conformationally-closed form. A recent study showed that a covalently-cross-linked closed form of CPR (whose crystal structure was also reported) only supported 5% electron flux to cytochrome *c* relative to the unlinked CPR [26]. We have obtained the same result for a similarly cross-linked nNOSred (Y. Dai and D. J. Stuehr, unpublished observations). Thus, the assumption holds for CPR and nNOSred and we assume that it also holds for the other two flavoproteins, given their structural and mechanistic similarities. Secondly, we assume that the reduced FMN domain is very reactive toward cytochrome *c* once it becomes sufficiently unencumbered enough for its bound FMN_{hq} to come within a distance that allows fast ET to

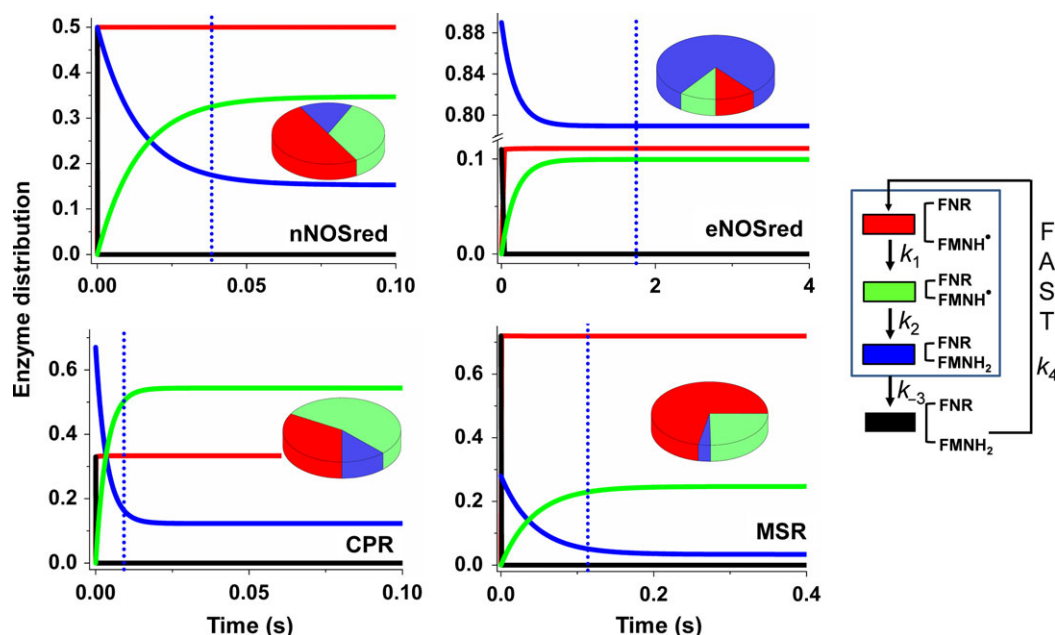


Fig. 5. Patterns of enzyme distribution versus reaction time in dual flavin enzymes. Rate pairs of conformational motion and interflavin electron transfer (obtained from the simulated best fit values) (Fig. 4) were used in each case to simulate and achieve experimentally obtained cytochrome *c* reduction rates. Lines indicate the relative concentrations of each enzyme species a-d (Fig. 1), with the total enzyme concentration being 1.0 and the concentration of enzyme species d + a set equal to 1.0 at $t = 0$ in the simulations. The blue dotted line marks the time required for the enzyme to reduce one equivalent of cytochrome *c*. Kinetic settings were: For nNOSred: $k_1 = k_3 = 53$, $k_2 = 22$; for eNOSred: $k_1 = k_3 = 5.0$, $k_1 = k_3 = 0.63$, $k_2 = 5$; for CPR: $k_1 = k_3 = 460$, $k_1 = k_3 = 230$, $k_2 = 52$; for MSR: $k_1 = k_3 = 8$, $k_1 = k_3 = 20.5$, $k_2 = 2.8$. Pie graphs show different species distributed at steady state. Color scheme for different species: black, species a; red, species b; green, species c; blue, species d.

cytochrome *c*. The cytochrome *c* reactivity of the reduced, isolated FMN domains of CPR and nNOS [37,42] are sufficiently reactive to support this assumption, and we assume that this is also the case for MSR and eNOS.

At equilibrium, the four reduced flavoproteins likely populate a myriad of closed and open forms that distribute across a conformational and energetic landscape, as described, for example, by Hay *et al.* [43]. Crystal structures of nNOSred and CPR illustrate their tightly closed forms [23,25]. More recent crystallographic, cryogenic, small-angle X-ray (SAXS) or neutron scattering (SANS) and solution NMR or EPR studies of CPR and its variants or of nNOS have identified conformationally-open forms and shown that multiple states are indeed populated at equilibrium [27,32,44–46]. The FMN domain in each of three open conformer crystal structures of CPR is sufficiently unencumbered to engage in fast ET with cytochrome *c*. However, it is unclear which of these open conformations may actually form during catalysis, or how well they each might cycle to participate in steady-state electron flux to cytochrome *c*. Obviously, minimal conformational changes that would still allow

ET from FMN_{hq} to cytochrome *c* would be likely to enable the fast conformational cycling and fast electron flux that is seen in CPR. In contrast, the more extended open conformers may participate poorly, given that these conformers were observed in the structure of CPR variants that display very low steady-state cytochrome *c* reductase activity [27]. Populating extended conformations or undergoing conformational relaxations back to closed conformations have been suggested to be gradual processes [47,48] and possibly artifacts of dilution [30,49] or of the long equilibration times that enzyme molecules experience when being readied for laboratory studies. We do not know whether such relaxations redistributed the conformationally-open or closed forms in the fully-reduced flavoproteins prior to our stopped-flow mixing experiments. However, the traces in Fig. 2 may suggest that this did not happen to any significant extent. The cytochrome *c* reductase activities calculated from tangents drawn to the stopped-flow traces in Fig. 2 matched fairly well with the steady-state activities determined for MSR, CPR, eNOSred and nNOSred in standard activity assays (Table 3) that were run over several minutes and did not involve a pre-reduction of the

steady state activity measured by the standard method.

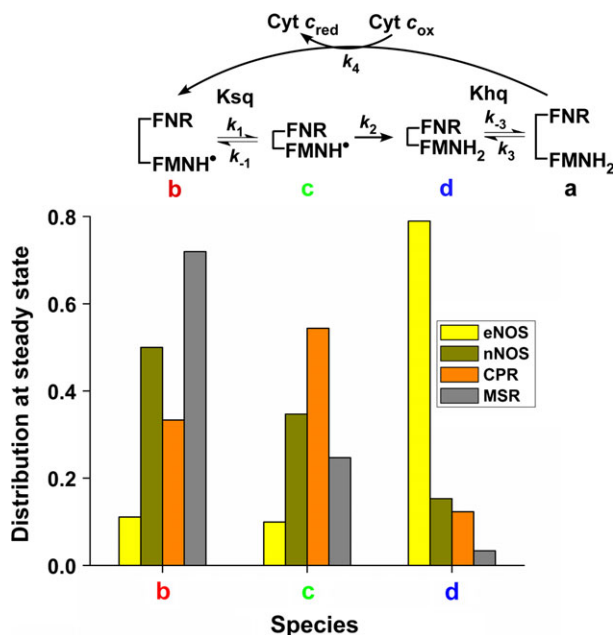


Fig. 6. The steady state distributions of different species among the four flavoproteins. Build up of different species at steady state. Build up of the conformationally open FMN_{hq} species (species a) is essentially nil in all enzymes because it reacts so quickly with the excess cytochrome c.

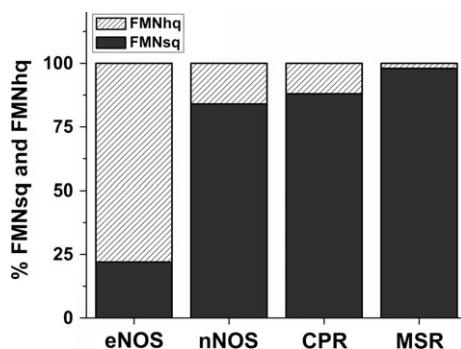


Fig. 7. Percentage proportion of FMN_{sq} versus FMN_{hq} present in each enzyme during its steady state reaction with cytochrome c.

enzymes before their activity was measured. Indeed, the kinetic traces in Fig. 2 imply that each fully-reduced flavoprotein quickly achieved the conformational and redox cycling that normally occurs during its steady-state reaction with cytochrome *c*. If instead, a significant relaxation to poorly-cycling open conformers or a relaxation to closed conformers had occurred during the time required to prepare the enzymes for the stopped-flow experiments, then we would expect a mismatch between the tangent-based activity derived from the traces in Fig. 2 and the

Possible relationships between the enzyme redox state and conformational behaviors

Studies with CPR have suggested that the flavin reduction may impact the conformational setpoint by shifting CPR to favor more open forms [44,45,50]. NADPH binding site occupancy can also impact conformational behaviors of CPR and nNOS [13,15,30,35,40,41,50,51]. Moreover, the interflavin ET step that generates FMN_{hq} (k_2 in Fig. 1) has been suggested to gate a subsequent conformational opening step that frees the reduced FMN_{hq} domain in CPR (k_{-3} in Fig. 1) [41,43,52]. These concepts are fundamentally important but are not directly addressed by our results because we only investigated the conformational behaviors of the fully-reduced flavoproteins. However, some of our observations may shed some light. First, we found that none of the four flavoproteins existed in a completely open conformation when they were fully-reduced (i.e. when they contained two-electron reduced (hydroquinone) FAD, FMN_{hq} and bound NADPH). Indeed, our evidence suggests that two of the four (eNOSred and CPR) exist predominantly in their closed conformations even when fully reduced. This implies that reduction to create FMN_{hq} has at most a partial and variable capacity to trigger conformational opening among the four flavoproteins. This can be viewed within the context of recent SAXS and SANS studies on CPR, which reported that a two-electron reduction of the fully-oxidized enzyme caused some opening and stabilized approximately 50% of the enzyme in an open conformation [45]. Note that CPR in the two-electron reduced state would predominantly contain FAD semiquinone (FAD_{sq}) and FMN_{sq}, and so the conformational change that was reported in their study was predominantly associated with the transition of FMN_{ox} to FMN_{sq} in CPR. The study did not address what effect, if any, that further reduction of FMN_{sq} to FMN_{hq} might cause on the CPR conformation. Given that our study estimated that fully-reduced CPR is one-third open and two-thirds closed, our results imply there may be no further opening upon reduction of its FMN_{sq} to FMN_{hq}. Second, a comparison of the best-fit rate estimate that we derived for the interflavin ET step (k_2) and the rate for the conformational opening step of each reduced flavoprotein (k_{-3}) shows that no correlation exists between these two rates (Table 3). For example, the estimated rate of interflavin ET in eNOSred is eight-fold faster than its estimated rate of

conformational opening. For MSR and CPR, the situation is reversed, and their estimated rates of conformational opening are seven and four times faster than their estimated rates of interflavin ET, respectively. In contrast, the estimated conformational closing rates of the FMN_{sq}-containing species (k_1 in Fig. 1), which is the step that precedes the interflavin ET are more similar to the estimated rates of interflavin ET in eNOSred and MSR (Table 3). Further investigation is clearly warranted but, in any case, the present study suggests that one need not invoke a conformational sensitivity toward the FMN_{sq} and FMN_{hq} redox states, or a gating of the FMN domain motion to the interflavin ET step, in order to model electron flux through these flavoproteins.

Structural considerations and possible basis for different electron flux among the diflavin reductases

Perhaps the most remarkable findings suggested by the present study is that the four diflavin reductases differ so widely in their conformational equilibrium setpoints and also exhibit a two-order of magnitude range in their rates of FMN domain conformational switching. We found that MSR and eNOSred have conformational equilibrium setpoints that lie on either side of the optimum setting ($K_{hq} = 1$ being approximately optimal in this model) [15,34] and their K_{sq} and K_{hq} setpoints therefore help to limit their electron flux as a result of an imbalance between their conformational closing and opening rates. However, on balance, it is their slow rates of conformational switching that present the biggest barrier to their electron flux. Consider that the K_{hq} setpoint of CPR is also suboptimal but its much faster rates of conformational switching supercede this limitation. Interestingly, our results predict that slightly shifting the K_{hq} of CPR toward its open reactive form would increase its activity above wild-type enzyme, and we suspect that this effect might explain a recently-characterized CPR point mutant with a higher than normal activity [45].

The best-fit rates we derived for CPR conformational switching (230 and 460 s⁻¹) are in the middle to high range of similar switching rates reported in other multidomain redox enzymes [28,41,51,53], whereas the rates we estimated for nNOSred, MSR and eNOSred are in the lower to extreme lower end of the range. This suggests that ‘suppressive’ features exist in these three flavoproteins that slow down their rates of conformational cycling relative to CPR or other multidomain redox enzymes and, for MSR and eNOSred, may also give them suboptimal conformational K_{hq} settings, thus preventing them from achieving a faster electron flux as is seen for CPR. What might these features be? We know that calmodulin binding to nNOSred boosts its cytochrome *c* reductase activity to the level of CPR [15,36,40,54–58] and thus calmodulin likely relieves the suppressive features that are present in the nNOSred [15,40,56,59].

Regarding the protein structural features held in common among diflavin reductases, we may consider the FNR FMN domain linker that is directly involved in conformational switching and differs considerably with regard to its length and amino acid sequence [18,19,25,27,60] and also consider the domain domain interface. We have examined the available structural information on dual-flavin reductases. The structure of the diflavin module has been elucidated for nNOS and CPR. We used the Protein Data Bank (PDB) files [1TLL](#) [25] for nNOS and [1AMO](#) [23] for CPR. Because the structures of the complete diflavin module are not available for eNOS and MSR, we have built structural models using available modeling servers (See Experimental procedures).

The analysis of the FNR/FMN domain interfaces in the structures and models is shown in Table 4. In summary, it appears that the interface area between FNR and FMN domains is very similar for nNOS, eNOS and CPR (approximately 2500 Å²), whereas the interface is smaller in the case of MSR (approximately 2000 Å²). The arrangement of the FNR and FMN domains appears to be very similar in all cases (Fig. 8) and the changes in surface area can be ascribed to the

Table 4. Properties of the FNR/FMN domain interaction surfaces of selected diflavin reductases.

Protein	nNOS	eNOS	CPR	MSR	MSR
PDB file	1TLL	Model (template: 1TLL)	1AMO	Model (template: 1AMO)	Model (template: 1TLL)
Total interface area (Å ²)	2510.9	2502.2	2501.5	1970.4	1980.8
% Charged residues	40.0	47.4	57.1	52.9	31.2
Nonbonded contacts	83	101	84	134	60
Hydrogen bonds	2	3	5	2	0
Salt bridges	1	1	4	2	1

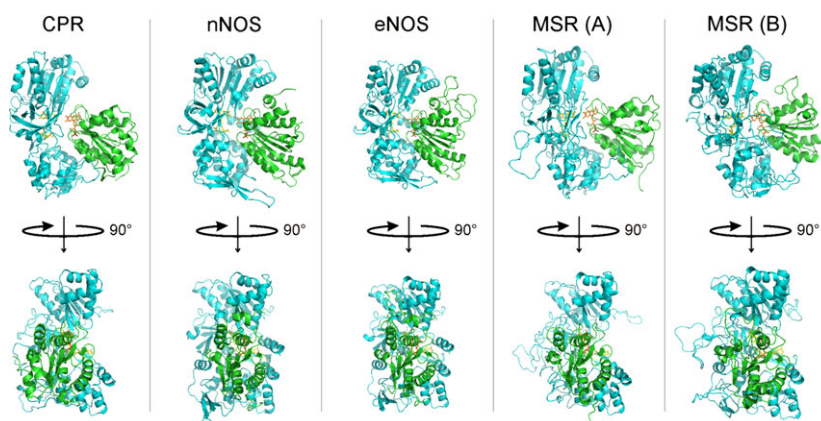


Fig. 8. Crystal structures and structure based models of flavoproteins. We used 1AMO for rat cytochrome P450 reductase and 1TLL for rat nNOS. The available structure of rat nNOS (1TLL) was used as template for the bovine eNOS model. We built two different models for methionine synthase reductase using either nNOS (1TLL) or cytochrome P450 reductase (1AMO) structures as templates. Upper panels: side view of structure. Lower panels: top view of structure. FNR domain is shown in blue; FMN domain is shown in green; FAD (yellow) and FMN (orange) are shown as sticks.

presence of 'extra' elements in NOS and CPR compared to MSR. NOS proteins include an additional autoinhibitory helix element in their FMN domain that is known to modulate the interaction with CaM (amino acids 836–849 in nNOS and 609–621 in eNOS) [25,61] and also contain a C-terminal extension in their FNR domain that modulates the FMN-FNR domain interaction and CaM response [39]. Both elements contribute to their FMN-FNR interface. In the case of CPR, the FMN domain possesses an extra helical segment (amino acids 67–78) that interacts with the FNR domain, including the formation of a salt bridge between amino acids Arg⁷⁸ of the FMN domain and Asp³⁵² of the FNR domain. The MSR sequence does not incorporate any of these elements, and thus its resulting interaction area is approximately 500 Å² smaller than for NOS or CPR (Table 4).

MSR has a long hinge region (approximately 80 amino acids) between the FMN and FNR domains, different from the shorter hinges (14–25 amino acids) in NOS or CPR. Due to its location in the primary structure, it is reasonable to think that this hinge region could mediate additional FMN/FNR domain interactions in MSR. However, some secondary evidence suggests that this may not be the case. First, crystallization of the hinge and FNR portion of MSR (residues 166–698) was only able to determine the structure of the portion of the hinge between amino acids 217 and 247 [62]. This section stretches away from the putative location of the FMN module and is unlikely to contribute to FNR-FMN binding; the region between residues 166 and 217 was too flexible for the structure to be determined. Secondly, difficulty

in obtaining a crystal structure of the whole MSR protein also points towards a transient, unstable FNR-FMN complex in MSR. Thirdly, our experimental data indicate that an open conformation is prevalent in MSR (Table 2). It is possible that the presence of the FMN module helps to arrange the hinge region in a more stable structure that provides additional stability to the FMN-FNR module, although the evidence discussed above appears to argue against this hypothesis. In the absence of more structural data, the contribution of this sequence to interdomain binding remains an open question.

As noted previously, NOS and CPR include a shorter (approximately 14 amino acids in CPR and 25 amino acids in NOS), flexible hinge region between the FMN and FNR domains. The composition of the hinge modulates the equilibrium between open and closed conformations, as shown by studies on CPR [27,63] and NOS [60,64]. Due to the flexibility of these regions, they do not appear in the crystal structures available, and we excluded the sequences from our analysis in the modeled structures. As discussed in the case of MSR, the hinge can contribute to the energy of the closed conformation. However, we expect that contribution to be minor in terms of complex stabilization because these fragments do not form a fixed, 'clamp' structure between the FNR and FMN domains, as confirmed by the crystallography experiments. In turn, they appear to operate on the conformational equilibrium by limiting the degrees of freedom of the open conformations [15,27,60,63,64]. In this way, the effect of the hinges will be more related to the kinetics of the conformational changes between

open and closed conformations, whereas the equilibrium setpoint between both conformations will be more related to the strength of the interaction between the FNR and FMN domains in the closed conformation. Thus, we consider that the omission of the hinge fragments from the interface analysis will not modify the conclusions of the present study.

The comparison of the binding interactions for the structures and models indicates that the number of hydrogen bonds plus salt bridges is higher for eNOS ($n = 4$) and CPR ($n = 9$) than for nNOS ($n = 3$) (Table 4). Qualitatively, and considering that the stability of the complex will be mainly determined by the interface area, the stability of the 'closed' conformations could be ordered as $\text{eNOS} \approx \text{CPR} > \text{nNOS} > \text{MSR}$. We observe that this ranking correlates with the observed amount of 'closed' conformation for each fully-reduced enzyme (Table 2). Clearly, how these and other structural features influence interflavin ET, conformational K_{hq} setpoints, and switching rates remains a topic of ongoing study.

In sum, the present study provides the first comparative estimates of the conformational equilibria setpoints, interflavin ET rates and conformational switching rates in four mammalian dual-flavin reductases, and shows how differences in these parameters can explain their widely different capacities to support electron flux from NADPH to cytochrome *c*.

Experimental procedures

Steady-state cytochrome *c* reduction assays

Cytochrome *c* reductase activity was determined at 25 and 10 °C by monitoring A_{550} and using an extinction coefficient of $\epsilon_{550} = 21 \text{ mM}^{-1} \cdot \text{cm}^{-1}$ as described previously [17,27,35,36].

Reaction of fully reduced proteins with excess cytochrome *c*

The rate of reduction of excess cytochrome *c* by fully reduced proteins was measured in the stopped flow instrument under anaerobic conditions at 10 °C as described previously [35,36]. The nNOSred or eNOSred (10–12 μM) proteins in 40 mM 4 (2-hydroxyethyl) 1-piperazinepropane sulfonic acid buffer (pH 7.6) with 10% glycerol and 150 mM NaCl containing EDTA (2 mM) were fully reduced by titrating them with anaerobic sodium dithionite solution. We used 0.1 M potassium phosphate buffer (pH 7.4) with 10% glycerol for CPR and MSR proteins, otherwise keeping the rest of the procedure the same as that used for the two NOSred proteins. An anaerobic solution of each

fully reduced protein containing NADPH (200 μM) was mixed with an anaerobic solution of cytochrome *c* (100 μM) while monitoring the changes in A_{550} . Initially, the solution of cytochrome *c* was mixed with anaerobic buffer alone to obtain the initial A_{550} reading at $t = 0$. All mixing reactions were repeated consecutively six to eight times, and then the individual kinetic traces were averaged. The entire analysis was then repeated using a separately purified batch of each enzyme. In the reactions of reduced enzyme with cytochrome *c*, a linear regression analysis of late points in the traces and/or numeric derivatives of the traces were run to determine the deflection points separating the early burst of fast reacting and late slow reacting phases (see Results).

Simulation of the kinetic traces of fully reduced flavoproteins with excess cytochrome *c*

We used the computer software GEPASI, version 3.30 [65] to simulate the experimental electron flux to cytochrome *c* using the kinetic model outlined in Fig. 1. Details of this type of simulations have been reported previously [34,35]. Here, we set the reaction rate with cytochrome *c* (k_4 in the kinetic model) at 225 s^{-1} in all cases, based on a reported second order rate constant ($4.5 \times 10^6 \text{ M}^{-1} \cdot \text{s}^{-1}$) for the reaction of cytochrome *c* with the reduced conformationally open nNOSred, or with its reduced isolated FMN domain, at 10 °C [36,37,40]. Values for each of the four conformational rates (k_1 , k_{-1} , k_3 and k_{-3}) and the interflavin electron transfer rate (k_2) were input into the software. Each simulated reaction began with 100% of the enzyme in the fully reduced state (represented by species d and a in Fig. 1). The initial concentrations of species d and a were determined based on the experimentally obtained K_{hq} values. Inputs that satisfy the observed conformational equilibrium constant are used first and then refined in an iterative process using the time of first turnover and overall best fit of the kinetic trace as criteria to identify the best fit rates for FMN conformational motion and interflavin electron transfer.

Structure-based analysis of the domain interfaces

Existing PDB structures were used when available. We used 1TLL [25] for rat nNOS and 1AMO [23] for rat CPR. In the case of bovine eNOS and human MSR, structures were modeled using the Swiss Model Server [66]. The available structure of rat nNOS (1TLL) was used as template for the bovine eNOS model, being by far the template with the highest sequence identity. In the case of human MSR, a structure for the FNR domain is available [62], although the structure of the FMN domain has not been determined. Because both nNOS and CPR have significant sequence identity (approximately 33%) to MSR, we built two different models for MSR using either nNOS or CPR structures as templates.

The interface area and the atom interactions for each structure were calculated using the 2P2I server [67]. The output of the 2P2I server was also used to compile the tables of atom and residue contacts (Supplemental Table S1).

The definition of the FNR like and FMN domains for each protein was: rat nNOS, FMN domain amino acids 750 942, FNR domain amino acids 968 1413; CPR, FMN domain amino acids 64 235, FNR domain amino acids 243 678; eNOS, FMN domain amino acids 519 721, FNR domain amino acids 728 1180 (segment 722 727 removed for calculations); MSR/ITLL model, FMN domain amino acids 6 162, FNR domain amino acids 210 697 (segment 163 209 removed for calculations); MSR/1AMO model, FMN domain amino acids 2 162, FNR domain amino acids 210 698 (segment 163 209 removed for calculations). In the available structures of CPR and nNOS, the hinge fragments between the FNR and FMN domains are too flexible and not visible in the crystal structure (236 242 in CPR; 952 958 in nNOS). We considered that the structure of the homologous fragment in the eNOS model (722 727) was not reliable and was removed before analysis. In the case of MSR, the polypeptide including the FNR domain and the hinge domain (amino acids 166 698) has been analyzed but only the fragment between amino acids 217 and 698 yield a crystal structure [62]. We therefore excluded the fragment from our study. Comparison of the MSR models with the available MSR structure [62] indicates that the estimated location of the segments between amino acids 210 and 270 is not consistent with the reported structure. Nevertheless, we did not remove these fragments because they are far from the FNR/FMN domain interface and do not modify our calculations. The PDB files used for the analysis are available in the supplementary materials.

Acknowledgements

We thank Deb Durra for technical assistance and Dr David Coe for performing the initial experiments with CPR. We thank Dr Ruma Banerjee for the MSR bacterial expression construct. This work was supported by National Institutes of Health Grants GM51491 and HL076491 to D.J.S.

Author contribution

MMH and MB designed and performed the experiments and analysed the data. JT did the structural analyses of proteins. CTK performed the steady state assays and helped in preparing first draft of the manuscript. NMP and SCI provided the purified CPR proteins. MMH, MB and JT drafted the paper. LW analysed the data. DJS designed the research, analysed the data and wrote the final paper.

References

- 1 Aigrain L, Fatemi F, Frances O, Lescop E & Truan G (2012) Dynamic control of electron transfers in diflavin reductases. *Int J Mol Sci* **13**, 15012–15041.
- 2 De Colibus L & Mattevi A (2006) New frontiers in structural flavoenzymology. *Curr Opin Struct Biol* **16**, 722–728.
- 3 Iyanagi T (2005) Structure and function of NADPH cytochrome P450 reductase and nitric oxide synthase reductase domain. *Biochem Biophys Res Commun* **338**, 520–528.
- 4 Joosten V & van Berkel WJ (2007) Flavoenzymes. *Curr Opin Chem Biol* **11**, 195–202.
- 5 Gomez Moreno C (2009) New roles of flavoproteins in molecular cell biology. *FEBS J* **276**, 4289.
- 6 Iyanagi T, Xia C & Kim JJ (2012) NADPH cytochrome P450 oxidoreductase: prototypic member of the diflavin reductase family. *Arch Biochem Biophys* **528**, 72–89.
- 7 Porter TD & Kasper CB (1986) NADPH cytochrome P 450 oxidoreductase: flavin mononucleotide and flavin adenine dinucleotide domains evolved from different flavoproteins. *Biochemistry* **25**, 1682–1687.
- 8 Porter TD (1991) An unusual yet strongly conserved flavoprotein reductase in bacteria and mammals. *Trends Biochem Sci* **16**, 154–158.
- 9 Murataliev MB, Feyerisen R & Walker FA (2004) Electron transfer by diflavin reductases. *Biochim Biophys Acta* **1698**, 1–26.
- 10 Iyanagi T & Mason HS (1973) Some properties of hepatic reduced nicotinamide adenine dinucleotide phosphate cytochrome c reductase. *Biochemistry* **12**, 2297–2308.
- 11 Vermilion JL & Coon MJ (1978) Purified liver microsomal NADPH cytochrome P 450 reductase. Spectral characterization of oxidation reduction states. *J Biol Chem* **253**, 2694–2704.
- 12 Shen AL, O'Leary KA & Kasper CB (2002) Association of multiple developmental defects and embryonic lethality with loss of microsomal NADPH cytochrome P450 oxidoreductase. *J Biol Chem* **277**, 6536–6541.
- 13 Daff S (2010) NO synthase: structures and mechanisms. *Nitric Oxide* **23**, 1–11.
- 14 Feng C (2012) Mechanism of nitric oxide synthase regulation: electron transfer and interdomain interactions. *Coord Chem Rev* **256**, 393–411.
- 15 Stuehr DJ, Tejero J & Haque MM (2009) Structural and mechanistic aspects of flavoproteins: electron transfer through the nitric oxide synthase flavoprotein domain. *FEBS J* **276**, 3959–3974.
- 16 Leclerc D, Wilson A, Dumas R, Gafuik C, Song D, Watkins D, Heng HH, Rommens JM, Scherer SW, Rosenblatt DS *et al.* (1998) Cloning and mapping of a cDNA for methionine synthase reductase, a

- flavoprotein defective in patients with homocystinuria. *Proc Natl Acad Sci USA* **95**, 3059–3064.
- 17 Olteanu H & Banerjee R (2001) Human methionine synthase reductase, a soluble P 450 reductase like dual flavoprotein, is sufficient for NADPH dependent methionine synthase activation. *J Biol Chem* **276**, 35558–35563.
 - 18 Wolthers KR & Scrutton NS (2007) Protein interactions in the human methionine synthase methionine synthase reductase complex and implications for the mechanism of enzyme reactivation. *Biochemistry* **46**, 6696–6709.
 - 19 Paine MJ, Garner AP, Powell D, Sibbald J, Sales M, Pratt N, Smith T, Tew DG & Wolf CR (2000) Cloning and characterization of a novel human dual flavin reductase. *J Biol Chem* **275**, 1471–1478.
 - 20 Ostrowski J, Barber MJ, Rueger DC, Miller BE, Siegel LM & Kredich NM (1989) Characterization of the flavoprotein moieties of NADPH sulfite reductase from *Salmonella typhimurium* and *Escherichia coli*. Physicochemical and catalytic properties, amino acid sequence deduced from DNA sequence of *cysJ*, and comparison with NADPH cytochrome P 450 reductase. *J Biol Chem* **264**, 15796–15808.
 - 21 Munro AW, Leys DG, McLean KJ, Marshall KR, Ost TW, Daff S, Miles CS, Chapman SK, Lysek DA, Moser CC *et al.* (2002) P450 BM3: the very model of a modern flavocytochrome. *Trends Biochem Sci* **27**, 250–257.
 - 22 Munro AW, Girvan HM & McLean KJ (2007) Cytochrome P450 redox partner fusion enzymes. *Biochim Biophys Acta* **1770**, 345–359.
 - 23 Wang M, Roberts DL, Paschke R, Shea TM, Masters BS & Kim JJ (1997) Three dimensional structure of NADPH cytochrome P450 reductase: prototype for FMN and FAD containing enzymes. *Proc Natl Acad Sci USA* **94**, 8411–8416.
 - 24 Xia C, Panda SP, Marohnic CC, Martasek P, Masters BS & Kim JJ (2011) Structural basis for human NADPH cytochrome P450 oxidoreductase deficiency. *Proc Natl Acad Sci USA* **108**, 13486–13491.
 - 25 Garcin ED, Bruns CM, Lloyd SJ, Hosfield DJ, Tiso M, Gachhui R, Stuehr DJ, Tainer JA & Getzoff ED (2004) Structural basis for isozyme specific regulation of electron transfer in nitric oxide synthase. *J Biol Chem* **279**, 37918–37927.
 - 26 Xia C, Hamdane D, Shen AL, Choi V, Kasper CB, Pearl NM, Zhang H, Im SC, Waskell L & Kim JJ (2011) Conformational changes of NADPH cytochrome P450 oxidoreductase are essential for catalysis and cofactor binding. *J Biol Chem* **286**, 16246–16260.
 - 27 Hamdane D, Xia C, Im SC, Zhang H, Kim JJ & Waskell L (2009) Structure and function of an NADPH cytochrome P450 oxidoreductase in an open conformation capable of reducing cytochrome P450. *J Biol Chem* **284**, 11374–11384.
 - 28 Laursen T, Jensen K & Moller BL (2011) Conformational changes of the NADPH dependent cytochrome P450 reductase in the course of electron transfer to cytochromes P450. *Biochim Biophys Acta* **1814**, 132–138.
 - 29 Meints CE, Gustafsson FS, Scrutton NS & Wolthers KR (2011) Tryptophan 697 modulates hydride and interflavin electron transfer in human methionine synthase reductase. *Biochemistry* **50**, 11131–11142.
 - 30 Pudney CR, Heyes DJ, Khara B, Hay S, Rigby SE & Scrutton NS (2012) Kinetic and spectroscopic probes of motions and catalysis in the cytochrome P450 reductase family of enzymes. *FEBS J* **279**, 1534–1544.
 - 31 Wolthers KR & Scrutton NS (2004) Electron transfer in human methionine synthase reductase studied by stopped flow spectrophotometry. *Biochemistry* **43**, 490–500.
 - 32 Aigrain L, Pompon D, Morera S & Truan G (2009) Structure of the open conformation of a functional chimeric NADPH cytochrome P450 reductase. *EMBO Rep* **10**, 742–747.
 - 33 Ghosh DK, Ray K, Rogers AJ, Nahm NJ & Salerno JC (2012) FMN fluorescence in inducible NOS constructs reveals a series of conformational states involved in the reductase catalytic cycle. *FEBS J* **279**, 1306–1317.
 - 34 Haque MM, Kenney C, Tejero J & Stuehr DJ (2011) A kinetic model linking protein conformational motions, interflavin electron transfer and electron flux through a dual flavin enzyme simulating the reductase activity of the endothelial and neuronal nitric oxide synthase flavoprotein domains. *FEBS J* **278**, 4055–4069.
 - 35 Haque MM, Bayachou M, Fadlalla MA, Durra D & Stuehr DJ (2013) Charge Pairing Interactions Control the Conformational Setpoint and Motions of the FMN Domain in Neuronal Nitric Oxide Synthase. *Biochem J* **450**, 607–617.
 - 36 Ilagan RP, Tiso M, Konas DW, Hemann C, Durra D, Hille R & Stuehr DJ (2008) Differences in a conformational equilibrium distinguish catalysis by the endothelial and neuronal nitric oxide synthase flavoproteins. *J Biol Chem* **283**, 19603–19615.
 - 37 Ilagan RP, Tejero J, Aulak KS, Ray SS, Hemann C, Wang ZQ, Gangoda M, Zweier JL & Stuehr DJ (2009) Regulation of FMN subdomain interactions and function in neuronal nitric oxide synthase. *Biochemistry* **48**, 3864–3876.
 - 38 Konas DW, Zhu K, Sharma M, Aulak KS, Brudvig GW & Stuehr DJ (2004) The FAD shielding residue Phe1395 regulates neuronal nitric oxide synthase catalysis by controlling NADP⁺ affinity and a conformational equilibrium within the flavoprotein domain. *J Biol Chem* **279**, 35412–35425.
 - 39 Tiso M, Tejero J, Panda K, Aulak KS & Stuehr DJ (2007) Versatile regulation of neuronal nitric oxide

- synthase by specific regions of its C terminal tail. *Biochemistry* **46**, 14418–14428.
- 40 Craig DH, Chapman SK & Daff S (2002) Calmodulin activates electron transfer through neuronal nitric oxide synthase reductase domain by releasing an NADPH dependent conformational lock. *J Biol Chem* **277**, 33987–33994.
 - 41 Gutierrez A, Paine M, Wolf CR, Scrutton NS & Roberts GC (2002) Relaxation kinetics of cytochrome P450 reductase: internal electron transfer is limited by conformational change and regulated by coenzyme binding. *Biochemistry* **41**, 4626–4637.
 - 42 Grunau A, Paine MJ, Ladbury JE & Gutierrez A (2006) Global effects of the energetics of coenzyme binding: NADPH controls the protein interaction properties of human cytochrome P450 reductase. *Biochemistry* **45**, 1421–1434.
 - 43 Hay S, Brenner S, Khara B, Quinn AM, Rigby SE & Scrutton NS (2010) Nature of the energy landscape for gated electron transfer in a dynamic redox protein. *J Am Chem Soc* **132**, 9738–9745.
 - 44 Ellis J, Gutierrez A, Barsukov IL, Huang WC, Grossmann JG & Roberts GC (2009) Domain motion in cytochrome P450 reductase: conformational equilibria revealed by NMR and small angle x ray scattering. *J Biol Chem* **284**, 36628–36637.
 - 45 Huang WC, Ellis J, Moody PC, Raven EL & Roberts GC (2013) Redox linked domain movements in the catalytic cycle of cytochrome p450 reductase. *Structure* **21**, 1581–1589.
 - 46 Persechini A, Tran QK, Black DJ & Gogol EP (2013) Calmodulin induced structural changes in endothelial nitric oxide synthase. *FEBS Lett* **587**, 297–301.
 - 47 Leys D, Basran J, Talfournier F, Sutcliffe MJ & Scrutton NS (2003) Extensive conformational sampling in a ternary electron transfer complex. *Nat Struct Biol* **10**, 219–225.
 - 48 Toogood HS, Leys D & Scrutton NS (2007) Dynamics driving function: new insights from electron transferring flavoproteins and partner complexes. *FEBS J* **274**, 5481–5504.
 - 49 Brenner S, Hay S, Munro AW & Scrutton NS (2008) Inter flavin electron transfer in cytochrome P450 reductase effects of solvent and pH identify hidden complexity in mechanism. *FEBS J* **275**, 4540–4557.
 - 50 Pudney CR, Khara B, Johannissen LO & Scrutton NS (2011) Coupled motions direct electrons along human microsomal P450 Chains. *PLoS Biol* **9**, e1001222.
 - 51 Gutierrez A, Munro AW, Grunau A, Wolf CR, Scrutton NS & Roberts GC (2003) Interflavin electron transfer in human cytochrome P450 reductase is enhanced by coenzyme binding. Relaxation kinetic studies with coenzyme analogues. *Eur J Biochem* **270**, 2612–2621.
 - 52 Leferink NG, Pudney CR, Brenner S, Heyes DJ, Eady RR, Samar HS, Hay S, Rigby SE & Scrutton NS (2012) Gating mechanisms for biological electron transfer: integrating structure with biophysics reveals the nature of redox control in cytochrome P450 reductase and copper dependent nitrite reductase. *FEBS Lett* **586**, 578–584.
 - 53 Gutierrez A, Grunau A, Paine M, Munro AW, Wolf CR, Roberts GC & Scrutton NS (2003) Electron transfer in human cytochrome P450 reductase. *Biochem Soc Trans* **31**, 497–501.
 - 54 Abu Soud HM, Yoho LL & Stuehr DJ (1994) Calmodulin controls neuronal nitric oxide synthase by a dual mechanism. Activation of intra and interdomain electron transfer. *J Biol Chem* **269**, 32047–32050.
 - 55 Chen PF & Wu KK (2003) Structural elements contribute to the calcium/calmodulin dependence on enzyme activation in human endothelial nitric oxide synthase. *J Biol Chem* **278**, 52392–52400.
 - 56 Daff S (2003) Calmodulin dependent regulation of mammalian nitric oxide synthase. *Biochem Soc Trans* **31**, 502–505.
 - 57 Matsuda H & Iyanagi T (1999) Calmodulin activates intramolecular electron transfer between the two flavins of neuronal nitric oxide synthase flavin domain. *Biochim Biophys Acta* **1473**, 345–355.
 - 58 Wu PR, Kuo CC, Yet SF, Liou JY, Wu KK & Chen PF (2012) Lobe specific calcium binding in calmodulin regulates endothelial nitric oxide synthase activation. *PLoS One* **7**, e39851.
 - 59 Roman LJ & Masters BS (2006) Electron transfer by neuronal nitric oxide synthase is regulated by concerted interaction of calmodulin and two intrinsic regulatory elements. *J Biol Chem* **281**, 23111–23118.
 - 60 Haque MM, Panda K, Tejero J, Aulak KS, Fadlalla MA, Mustovich AT & Stuehr DJ (2007) A connecting hinge represses the activity of endothelial nitric oxide synthase. *Proc Natl Acad Sci USA* **104**, 9254–9259.
 - 61 Salerno JC, Harris DE, Irizarry K, Patel B, Morales AJ, Smith SM, Martasek P, Roman LJ, Masters BS, Jones CL *et al.* (1997) An autoinhibitory control element defines calcium regulated isoforms of nitric oxide synthase. *J Biol Chem* **272**, 29769–29777.
 - 62 Wolthers KR, Lou X, Toogood HS, Leys D & Scrutton NS (2007) Mechanism of coenzyme binding to human methionine synthase reductase revealed through the crystal structure of the FNR like module and isothermal titration calorimetry. *Biochemistry* **46**, 11833–11844.
 - 63 Grunau A, Geraki K, Grossmann JG & Gutierrez A (2007) Conformational dynamics and the energetics of protein ligand interactions: role of interdomain loop in human cytochrome P450 reductase. *Biochemistry* **46**, 8244–8255.

- 64 Haque MM, Fadlalla MA, Aulak KS, Ghosh A, Durra D & Stuehr DJ (2012) Control of electron transfer and catalysis in neuronal nitric oxide synthase (nNOS) by a hinge connecting its FMN and FAD NADPH domains. *J Biol Chem* **287**, 30105–30116.
- 65 Mendes P (1993) GEPASI: a software package for modelling the dynamics, steady states and control of biochemical and other systems. *Comput Appl Biosci* **9**, 563–571.
- 66 Biasini M, Bienert S, Waterhouse A, Arnold K, Studer G, Schmidt T, Kiefer F, Cassarino TG, Bertoni M, Bordoli L *et al.* (2014) SWISS MODEL: modelling protein tertiary and quaternary structure using evolutionary information. *Nucleic Acids Res* **42**, W252–W258.
- 67 Basse MJ, Betzi S, Bourgeas R, Bouzidi S, Chetrit B, Hamon V, Morelli X & Roche P (2013) 2P2Idb: a structural database dedicated to orthosteric modulation of protein-protein interactions. *Nucleic Acids Res* **41**, D824–D827.

Supporting information

Additional supporting information may be found in the online version of this article at the publisher's web site:

Table S1. Residue contacts in different dual-flavin enzymes. Models and PDB files used for the structural analyses.